SCALE-UP TESTS OF HIGH REGRESSION RATE LIQUEFYING HYBRID ROCKET FUELS

M. Arif Karabeyoglu*, Greg Zilliac†, Brian J. Cantwell‡, Shane De Zilwa§ and Paul Castelluci¶

Stanford University
Stanford, CA
and
NASA Ames Research Center
Moffet Field, Mountain View, CA

Abstract

Recent research at Stanford University has led to the identification of a class of paraffin-based fuels that burn at surface regression rates that are 3 to 4 times that of conventional hybrid fuels. The approach involves the use of materials that form a thin, hydro-dynamically unstable liquid layer on the melting surface of the fuel. Entrainment of droplets from the liquid-gas interface can substantially increase the rate of fuel mass transfer leading to much higher surface regression rates than can be achieved with conventional polymeric fuels. Thus, a high regression rate is a natural attribute of the fuel material and the use of oxidizing additives or other regression rate enhancement schemes is not required. The high regression rate hybrid removes the need for a complex multi-port grain and most applications up to large boosters can be designed with a single port configuration. The fuel contains no toxic or hazardous components and can be shipped by commercial freight as a non-hazardous commodity. At the present time, grains up to 8.4 inches in diameter and 45 inches long are fabricated in a general-purpose laboratory at Stanford University. To further demonstrate the feasibility of this approach, a series of scale-up tests with gaseous oxygen have been carried out using a new Hybrid Combustion Facility (HCF) at NASA Ames Research Center. The data from these tests are in agreement with the small scale, low pressure and low mass flux laboratory tests at Stanford and confirm the high regression rate behavior of the fuels at chamber pressures and mass fluxes representative of commercial applications.

Nomenclature

a:	Regression rate coefficient	m:	Length exponent
A_{or}, A_n:	Sonic orifice and nozzle throat diameters	$\dot{m}_{ox}$:	Oxidizer mass flow rate
c_d, c_D:	Discharge coefficients of sonic orifice and nozzle	$\dot{m}_{ox}^{ter}$:	Oxidizer mass flow rate at valve closing event
c_{ox}^*:	Characteristic velocity of ambient gaseous oxygen	n:	Flux exponent
c_{act}^*, c_{theo}^*:	Measured and theoretical characteristic velocities	O/F:	Oxidizer to fuel ratio
d_f, d_i:	Final and initial port diameters	P_c, P_f:	Chamber and feed system pressures
d_{vc}:	Port diameter at valve closing	$\dot{r}$:	Fuel regression rate
G_{ox}, G_{tot}:	Oxidizer and total mass fluxes	t_b:	Burn time
L_g:	Grain length	t_f:	Thrust termination time
		V_f:	Feed system volume
		ΔM_f:	Mass of burned fuel

* Research Associate, Dept. of Aeronautics and Astronautics, Stanford University, Member AIAA
† Research Scientist, NASA Ames Research Center, Member AIAA
‡ Professor, Dept. of Aeronautics and Astronautics, Stanford University, Fellow AIAA
§ NRC Post Doctoral Fellow, NASA Ames Research Center, Member AIAA
¶ Graduate Student, Dept. of Aeronautics and Astronautics, Stanford University, Member AIAA

ΔM_{ox} : Mass of oxidizer burned

r_f: Fuel density

h_c : Combustion efficiency

1) Introduction

The hybrid rocket has been known for over 50 years, but was not given serious attention until the 1960's. The primary motivation was the non-explosive character of the fuel, which led to safety in both operation and manufacture. The fuel could be fabricated at any conventional commercial site and even at the launch complex with no danger of explosion. Thus, a large cost saving could be realized both in manufacture and launch operation. Compared to a solid rocket the hybrid is much less sensitive to cracks and de-bonds in the propellant, has a higher specific impulse (Isp) and can be throttled including shutdown and restart on demand[1-4].

The hybrid enjoys several advantages over a liquid system. One of the main advantages is a reduced explosion hazard, since an intimate mixture of oxidizer and fuel is not possible. In addition, the hybrid rocket requires one rather than two liquid containment and delivery systems. The complexity is further reduced by omission of a regenerative cooling system for both the chamber and nozzle. A wide throttle range is relatively easy to achieve in a hybrid where throttling the oxidizer automatically throttles the fuel and there is no requirement to match the momenta of the dual propellant streams during the throttling operation. Throttling ratios up to 10:1 have been demonstrated in hybrid motors.

Lastly, the fact that the fuel is in the solid phase makes it very easy to add solid performance-enhancing materials such as aluminum. This enables the hybrid to gain a specific impulse (Isp) and density advantage over a comparable hydrocarbon fueled liquid system. Metal additives can be used to reduce the O/F ratio for maximum specific impulse thereby enabling a reduction in the required mass of liquid oxidizer.

The principal disadvantage of the conventional hybrid rocket is the inherent low burning rate due to the diffusive nature of the combustion process. Hence, traditional hybrid motor designs have required multi-port grain geometries to achieve the required thrust levels. However, recent research at Stanford University has led to the identification of a class of fast burning fuels that form a hydrodynamically unstable liquid layer over the their surface[5, 6, 7 and 8]. A theory that explains the behavior of liquefying fuels has been developed and been used to identify fuel properties that will produce droplet entrainment[8]. A fast burning paraffin-based fuel has been formulated and tested in a lab-scale motor at Stanford University. Regression rates 3 to 4 times higher than that of conventional hybrid fuels (i.e. hydroxyl-terminated polybutadiene, HTPB) have been observed[6 and 7].

In this paper, we start with a hybrid system design example in order to illustrate how the high regression rates simplify the design/fabrication process and improve system performance. Later we summarize various alternative techniques to enhance the regression rates of hybrid fuels and briefly explain the shortcomings of these methods. Finally, we discuss the scale-up testing program on paraffin-based fuels and the results obtained from the 7.5 inch diameter (i.e. grain outside diameter) tests conducted at the Hybrid Combustion Facility (HCF) of the NASA Ames Research Center.

2) Effect of Regression Rate on the Hybrid Motor Design

The importance of high regression rates can be best demonstrated through the design process of a real hybrid system. The selected design example is a space motor that would replace the solid rocket system ORBUS 21[9]. The objective of this exercise is to compare a conventional multi-port hybrid with a single-port, high regression rate design. The IUS motor ORBUS 21 contains 10,380 kg of solid propellant when it is fully loaded and delivers a total impulse of 28.4 M N-sec.

It is convenient to use the total propellant loading as the parameter that needs to be matched by the hybrid replacement candidates. For the purposes of this paper, the hybrid design will not be optimized to generate the maximum possible delta V. This complex task requires the estimation of the motor component masses and the overall system mass fraction for each configuration. In our study, we simply select the operational conditions that will be used uniformly for all configurations in order to make a fair comparison. A detailed internal ballistic design is performed for each system.

Two fuels that will be considered in this comparison are the fast burning paraffin-based fuel formulation, SP-1a and the conventional HTPB-based system which is one the fastest burning polymeric fuels reported in the literature. The calculations are based on the following conditions:

1) The oxidizer is liquid oxygen. The oxidizer mass flow rate is constant with a value of approximately 29.6 kg/sec for all motors.

2) Fuel densities for HTPB and paraffin grains are taken as 0.915 and 0.920 g/cm^3, respectively.

3) The initial oxidizer mass flux for all systems is 50 g/cm^2-sec. A variation of this parameter within a reasonable range did not alter the performance significantly.

4) The c* and nozzle efficiencies are taken as 0.95 and 0.98, respectively. Note that the effects of oxidizer to fuel ratio (O/F) shift and nozzle erosion are not included in these efficiency values. The reductions induced by these factors are accounted for in the ballistic code.

5) A web support with 64 mm thickness and 1.0 g/cm^3 of density is used in the calculations involving multi-port grains.

6) The regression rate expression for the paraffin-based and HTPB-based fuels are taken to be:

Paraffin-based (SP-1a)[#]: $\dot{r} = 0.488 G_{ox}^{0.62}$

HTPB-based[10]: $\dot{r} = 0.146 G_{ox}^{0.681}$

Note that the regression rate is in mm/sec and oxidizer mass flux is g/cm^2-sec.

7) The Wagon Wheel configuration studied in this paper is composed of 7 pie-shaped ports and a circular center port (7+1 design). The hydraulic diameters of the pie and circular ports are matched for equal burning.

8) Atmospheric pressure is assumed to be zero.

9) A constant nozzle erosion rate of 0.178 mm/sec is used in the calculations.

10) An initial chamber pressure of 34 atm (500 psi) and initial nozzle area ratio of 70 are used for all calculations.

The vacuum specific impulse as a function of the motor O/F ratio is plotted in Figure 1 for the two fuel systems with liquid oxygen. The figure shows that the paraffin-based fuel has a slightly better Isp performance because of the higher hydrogen to carbon ratio and it reaches its peak at an O/F of roughly 2.7 as opposed to 2.5 for the HTPB system. This information is used to select the operational O/F ratio for each configuration.

We have identified three systems that demonstrate the effect of regression rate on the motor design: 1) HTPB-based single circular port, 2) Paraffin-based single circular port and 3) HTPB-based wagon wheel multi-port design. Figure 2 shows the schematics of the latter two of these configurations. The important design parameters for each configuration are summarized in Table 1. Note that, all three hybrid systems deliver higher total impulses compared to the solid rocket system ORBUS 21 and the paraffin-based system has a few seconds of Isp advantage over the HTPB systems.

The first point to make is that the HTPB-based single circular port motor is excessively long with a grain L/D of 12.22. This slow burning system is not practical because of the strict physical envelope requirements that exist for space engines and for many other applications. On the contrary, the fast burning single circular port system is one third of the length of the single-port HTPB unit, making it a much more attractive system[*]. The only way to match the grain L/D of the HTPB motor to the L/D of the fast burning hybrid is to adopt a multi-port design strategy. In fact for this particular case, it took a 7+1 wagon wheel design to match the L/D of the single port paraffin motor.

The penalties associated with such a complex multi-port design are severe:

- Excessive unburned mass fraction (i.e. typically in the 5% to 10% range).
- Complex design/fabrication, requirement for a web support structure.
- Compromised grain structural integrity, especially towards the end of the burn.
- Uneven burning of individual ports.
- Requirement for a substantial pre-combustion chamber or individual injectors for each port.

The potential problem areas introduced by the multi-port design strategy clearly highlights the necessity of a high regression rate fuel formulation in order to make the hybrid a viable alternative to the existing solid and liquid systems.

3) Approaches to High Regression Rate

Several methods to achieve high regression rates in hybrid rockets have been explored. Some of the most practical techniques can be listed as:

- Addition of oxidizing agents[11] or self decomposing materials in the hybrid fuel. This well known technique reverts to a quasi-solid

[#] See section 7 for a detailed discussion of the regression rate measurements.

[*] It is also worth noting that, if necessary, a further reduction in L/D can be achieved with the paraffin-based fuel by using a double-D or a four port grain design

design and eliminates the inherent safety characteristic of hybrid rockets.

- Addition of micron size metal additives. This is also a common technique that improves the fuel mass burning rate. The improvement is small (i.e. typically in the 10-20% range) and there are several shortcomings such as the increased vulnerability to instabilities due to the pressure dependent regression rate and increased environmental impact. This is a separate consideration from the addition of metal additives to increase fuel density, which is a useful improvement.
- Addition of nano-sized metal additives. This new approach improves the fuel mass burning rates up to 60%[12]. The major shortcomings are reduced Isp performance due to the metal oxide coating, complex processing due to hazardous material handling and high costs.
- Increasing the roughness of the burning surface by adding dispersed phase particles in the fuel that would burn at a different rate compared to the matrix material. This technique can only give a limited improvement and large solid particles injected in the gas stream reduce the efficiency of the system. The manufacturing costs would also increase.
- Using swirling injection of oxidizer. This method has a first-order effect on the regression rate as demonstrated by Knuth et al.[13]. They obtained up to a seven-fold increase in the regression rate of a HTPB/GOX hybrid using swirl oxidizer injection at the aft end of the motor. These results are promising although questions remain about the scalability to large motors and also the design impact of the complexity of the oxidizer injection technique.

Our approach involves the use of materials that form a thin, hydro-dynamically unstable liquid layer on the melting surface of the fuel. The instability of this layer driven by the oxidizer gas flow in the port leads to the entrainment of droplets into the gas stream, greatly increasing the overall fuel mass transfer rate. In effect, this mechanism acts like a continuous spray injection system distributed along the port with most of the fuel vaporization occurring around droplets convecting between the melt layer and the flame front. Conventional hybrids rely on evaporation and are subject to the so-called blocking effect where increased mass transfer from the fuel surface tends to reduce the heat transfer. Since droplet entrainment is not limited by diffusive heat transfer to the fuel from the combustion zone, this mechanism can lead to much higher surface regression rates than can be achieved with conventional polymeric fuels that rely solely on evaporation. Thus a high regression rate is a natural attribute of the fuel material avoiding the need for oxidizing additives or other complex regression rate enhancement schemes. As reported in Refs. 6 and 7, a factor of 3 to 4 increase in regression rate, in comparison with HTPB, has been measured experimentally.

4) Ames Hybrid Combustion Facility

To further demonstrate the feasibility and scalability of this approach, a new hybrid combustion test facility has been developed at NASA Ames Research Center. The Ames Hybrid Combustion Facility consists of an oxygen delivery system, a methane/oxygen based gas-gas ignition system and a combustion chamber as shown schematically in Figure 3. The oxygen delivery system is capable of delivering up to 16 kg/sec of ambient-temperature gaseous oxygen to the combustion facility at combustion chamber pressures that range between approximately 10 atm (150 psi) and 68 atm (1000 psi). During operation of the facility, a PID based feedback control system maintains a constant pressure upstream of the sonic orifice (by controlling the flow through a control valve) thereby establishing a constant oxygen mass flow rate that is decoupled from pressure fluctuations in the combustion chamber.

Combustion takes place in an insulated chamber that is roughly 47.3 in. long with an inside diameter of 7.672 in. and steel walls that are 1.25 in. thick. The fuel is contained in a paper phenolic cartridge that is inserted by removing threaded tie rods and sliding the combustion chamber components apart. During operation, gaseous oxygen (GOX) is fed to one end of the chamber and the exhaust exits through a convergent ATJ graphite nozzle on the opposite end of the chamber.

Standard measurements during a run of the facility include time histories of chamber pressure and oxygen mass flow rate. The chamber pressure is measured at the fore-end of the motor using a Kistler 601B transducer to resolve the fast varying component of the pressure and a Rosemount model 1151 pressure transducer for the DC component. Typical data sampling rate is 1000 Hz.

The facility became operational in September 2001 and since then, a series of tests have been undertaken on intermediate scale motors at pressures and mass fluxes representative of commercial applications. An image from the first test which was performed on September 24, 2001 is shown in Figure 4.

5) Grain Fabrication

Fuel grains are produced using a centrifugal casting process designed to produce crack-free and void-free grains. Paper phenolic tubes are used as the fuel cartridge. An annular, ATJ graphite insulator is bonded inside each end of tube, using a high-temperature epoxy. These insulators have a dual purpose. When casting fuel grains, the ATJ insulators mate with Teflon-coated, polyethylene plugs that seal-in the contents of the phenolic tube. When testing, the ATJ components mate with HCF insulators to prevent the external flow of combustion gases. The grains cast for the HCF tests include a blackening agent. The blackening agent, typically dye or carbon black, is necessary to ensure that radiative heat flux into the fuel grain is minimized. The fuel components are combined and heated in an 1800 W melting pot. Upon reaching 115 C, the melted fuel is thoroughly mixed and poured into the paper phenolic cartridge.

Depending on the grade of wax used, paraffin waxes can shrink up to 17% during solidification. To ensure that the solid fuel grain is void-free, centrifugal casting is employed. Centrifugal casting will also produce a grain that is well bonded to the casing with a single circular port of the desired diameter. Two O-ring sealed end plates are fitted to the tube allowing it to be mounted on a 2 Hp centrifuge. The centrifuge spins the tube about its axis at high speed (~1500 rpm) until the fuel has solidified after several hours. The contents of the tube, up to 20 kg of melted fuel, quickly achieve the system's rotational velocity. Once solidified, the fuel grain is removed from the centrifuge and inspected for defects. If a smaller port is required than can be achieved in a single pour, additional fuel is poured into the port and the process is repeated.

This casting process consistently produces well-bonded, single port fuel grains. The port surface is typically smooth, with less than 0.64 mm axial variation in diameter. About one out of every twenty-five grains will exhibit some minor cracking believed to be caused by thermal stresses. Although no grain has been cracked beyond usability, current efforts aim to explore the added benefits of annealing the fuel after casting to reduce internal stresses that develop during the solidification process. Finally, in contrast to a polymeric fuel, the residual paraffin-based fuel can be re-melted and included in a new casting thus eliminating waste.

6) Test Results

To date, approximately 200 tests have been carried out in the 2.38 inch (i.e. grain outside diameter) facility at Stanford University[6] and 29 tests in the 7.5 inch (i.e. grain outside diameter) facility at NASA Ames on the paraffin-based SP-1a fuel formulation. For all the tests described here, the oxidizer was gaseous oxygen. Results from a typical test are shown in Figure 5. Shown are the time histories for a nominal 68 atm (1000 psi) chamber pressure, 4 kg/sec oxidizer mass flow rate case (test 4P-03). The supply pressure is measured upstream of the sonic orifice. The oxidizer flow is initiated at approximately t=0 sec and ignition takes place at t=1.6 secs. At t=10.2 secs, the oxidizer shutoff valves are closed. As can be seen in the traces, thrust termination takes a few seconds because of the large volume of oxidizer in the lines between the shutoff valves and the combustion chamber

Out of the 29 motor tests with 28 paraffin-based fuel grains. 23 were used in data reduction to characterize the regression rate behavior of the paraffin based fuel formulation SP-1a (i.e. melting temperature of 69 C). The remaining 6 tests were not used for the regression rate evaluation purposes for the following reasons.

- 4F-2a-1 was shut down prematurely due to a software problem only a second after ignition.
- 4F-2a-2 used the same grain as 4F-2a-1. The goal of that test was to show the re-ignition capability. Since the pre-firing conditions of the grain were not known that successful run could not be used to evaluate the regression rate and the average oxidizer mass flux in the port.
- During run 4F-3, the stainless steel injector (used to replace a brass injector) ignited and started a metal fire at the fore end of the motor. We have decided against using the data from this run, due the unknown influence of the excess metallic mass generated at the fore-end on the regression rate characteristics of the fuel. Following this test a replacement injector made of copper was installed and this has fired successfully ever since.
- Tests 4L-06 and 4L-07 which were conducted with small port diameters (i.e. ~3.00" corresponding to 84% volumetric loading) resulted in excessive fuel regression rates. We believe that the excessive fuel mass generation observed in these tests is a result of the structural failure (i.e. possible crack formation) of the port internal surface. It can be shown that

for small port diameter to grain outside diameter ratios, the chamber pressure loading can generate very high tensile hoop stresses on the inner surface of the fuel grain. This fuel structural disintegration theory is supported by the low efficiencies estimated for these tests.

- During test 4L-11 the control system prematurely terminated the GOX flow. The burn time for this run is not adequate for accurate data reduction

7) Data Analysis

In the following sections the results obtained from the reduced test data will be discussed. The data reduction techniques are discussed in the Appendix and a summary of the test results is given in Tables 2 and 3. We concentrate on four key areas: 1) regression rate law determination, 2) motor efficiency evaluation, 3) ignition characteristics and 4) motor stability evaluation.

Regression Rate

Regression rate is the most important characteristic of a hybrid rocket fuel and a complete characterization of that quantity as a function of all the relevant operational variables of the hybrid motor is critical for the satisfactory design of a practical system.

Effect of Oxidizer Mass Flux: The averaged regression rates as a function of the averaged oxidizer mass fluxes for all the tests accepted for data reduction are shown in Figure 6. A curve fit to the data points (i.e. both lab-scale and larger scale) results in a mass flux exponent of 0.62 (i.e. see equation 2). Note that this value is small compared to the flux exponents commonly observed in classical propellants. This feature would reduce the extent of the O/F shift during the course of the motor operation and improve the Isp efficiency of the propulsion system.

Effect of Chamber Pressure: It has been determined that the effect of pressure on the regression rate is negligible (i.e. see Figure 7).

Effect of Grain Length: A significant effect of grain length on regression rate is not observed either going from the lab-scale to the HCF scale (i.e. factor of 7 in grain length) or upon going from one length to the other in the HCF testing (see Figure 8 for the latter result where grains of 33 and 45 inches in length are compared). For all the tests, the regression rate along the axis of the grain was quite uniform. Only a small increase (i.e. less than 10%) in the regression rate with increasing distance form the fore end has been observed.

Effect of Oxidizer to Fuel Ratio: A correction for the oxidizer to fuel ratio effect on the regression rate has been developed and applied to the lab-scale Stanford data and also to HFC data. The correction formula used in the calculations is

$$\frac{\bar{\dot{r}}}{a\bar{G}_{ox}^{n}L_{g}^{m}} = \left(\frac{1}{1+m}\right)\frac{1-n}{\left[\left(1+1/O/F\right)^{1-n}-1\right]O/F} \qquad (1)$$

where n is the flux exponent, a is the regression rate constant, m is the length exponent which is determined to be zero. This formula is derived by taking the space-average of the local regression rate expression. It has been observed that the correction based on the proceeding formula, which can be as large as 5-7 % in the most extreme cases, reduces the scatter in the regression rate data. Note that the data points shown in Figures 5, 6 and 7 are corrected for the O/F variation.

Based on the arguments of this section we suggest the following regression rate law for the paraffin-based fuel, SP-1a.

$$\bar{\dot{r}} = 0.488\,\bar{G}_{ox}^{0.62} \qquad (2)$$

The regression rate is in mm/sec and oxidizer mass flux is g/cm^2-sec. This formula can be used with reasonable accuracy within the motor O/F ratio range of 1.7-2.3. For O/F ratios significantly out of this range, we recommend the following equation, which includes the O/F correction.

$$\bar{\dot{r}} = \frac{0.163\ \bar{G}_{ox}^{0.62}}{\left[\left(1+1/O/F\right)^{0.38}-1\right]O/F} \qquad (3)$$

Efficiency:

Efficiencies based on c* are used for all motor tests. The efficiency values estimated for all motor tests are listed in Table 3 (i.e. see Appendix for the estimation method). It has been determined that the efficiency increases with increasing motor L* (due to increased residency time), increasing mass flux (due to reduced droplet size) and increasing motor O/F (possibly due to increased exposure of the droplets to the oxidizer). The delivered c* values calculated from data are plotted against motor O/F data in Figure 9. It can be seen from the figure that the

motor efficiencies improve with increasing O/F ratio and at an O/F ratio of 2.7, for which the theoretical Isp is maximized for the SP-1a propellant system, the motor efficiency range is 85-90%. Figure 10 shows the efficiency as a function of the motor L* for the motors running in the same O/F and mass flux range. Note that L* is defined as the ratio of the average combustion chamber volume to the average nozzle throat area. It is clear that the efficiency improves with increasing L*, indicating the encouraging result that larger scale systems would run at higher efficiencies. It should be noted that efforts specifically directed at improving the efficiency have not been attempted to-date in this program.

Ignition:

The ignition system is successfully tuned to achieve smooth reliable ignition for all the test conditions. Figures 5, 11 and 13 demonstrate the short ignition transient times and the small ignition overshoots typically achieved in our tests. The pressure time traces of all the motors generally showed the characteristics of classical hybrid rockets, a slight down slope with time due to the opening of the fuel port and nozzle throat. Towards the end of the run, nozzle erosion accelerates the time decay of chamber pressure slightly as can be seen in the figures.

Combustion Stability:

The facility is equipped with a fast response Kistler pressure transducer to permit spectral analysis of the pressure time history. Figure 11 shows data from one of the 20.4 atm (300 psi) chamber pressure runs. The rms of the pressure oscillations considered over one-second time intervals varied between 4 and 12 % of the mean pressure. The amplitude spectrum of the pressure fluctuations typically contained three distinct peaks at around 30 Hz, 100 Hz and 350 Hz as seen in Figure 12. The most dominant of these peaks is that at around 30 Hz, which is believed to be caused by a coupling between the delay in the boundary layer responding to any changes in mass flow and the thermal lag in the solid fuel. The mechanism of this instability is described by Karabeyoglu in Ref. 14. The peaks at around 100 and 350 Hz were associated with the bulk-mode and the acoustic half-wave in the combustion chamber, respectively. A more detailed description of these combustion oscillations will be presented in Ref. 15 by De Zilwa *et al.* (2003).

8) Conclusions

The design study on the ORBUS 21 replacement showed that the use of high regression rate fuel SP-1a, instead of the conventional HTPB, resulted in significant design simplifications and performance improvements. The fast burning non-toxic and non-hazardous fuel Sp-1a clearly presents a significant improvement over the conventional polymeric fuels.

The regression rates measured for paraffin-based fuel, SP1a, at two different scales (i.e. the 238 in. diameter Stanford motor and the 7 1/2-in. diameter HCF motor) are approximately 3 times larger than the regression rates of the classical hybrid fuel HTPB. The highest average and initial oxidizer fluxes tested so far in the program are 36.9 and 102.7 g/cm^2-sec, respectively. These values are well into the range of fluxes that would be used in an operational hybrid propulsion system. The highest chamber pressure tested so far is close to 68 atm (1000 psi). The mechanism leading to the high regression rate seems to be still active (as evidenced by the continuos nature of the regression rate curve) at those large fluxes, chamber pressures and for grains that are 7 times longer than the Stanford motor. No length or pressure dependency on the regression rate is observed.

The efficiencies of the motors tested range between 80 to 90 %. It appears that motors that are operated at higher fluxes tend to generate higher efficiencies. This observation is consistent with the theoretical understanding of the entrainment process, since at higher flux levels the droplet sizes that are entrained into the gas stream are predicted to be smaller. Efficiency also increases with increasing L* and motor O/F.

The test results, pressure time history and the regression rate behavior, are highly reproducible. In summary, the main conclusions from these scale-up tests are the following.

1) The high regression rate behavior observed in the small-scale tests at Stanford prevails when the motor is scaled up to chamber pressures and mass fluxes characteristic of operational systems. Moreover the regression rate data from large and small motors match quite well indicating that small-scale tests can be used to infer behavior of larger motors. This is extremely useful when it comes to developing the right fuel formulation for a given mission.

2) No length or pressure effect is observed on the regression rate. The regression rate along the axis of the grain has been observed to be uniform.

3) Paraffin-based fuels provide reliable ignition and stable combustion over the entire range of mass fluxes encountered (2-102 g/cm^2-sec).

4) The fuel exhibited good structural integrity over the range of chamber pressures used 10-68 atm (150-1000psi).

9) Acknowledgement

This work was carried out under cooperative agreements NAG3-2615 with the NASA Glenn Research Center and agreements NCC2-1172 and NCC2-1300 with the NASA Ames Research Center.

10) References

1. Marxman G. A., C. E. Wooldridge and R. J. Muzzy, "Fundamentals of Hybrid Boundary Layer Combustion", Progress in Astronautics and Aeronautics, Vol.15, 1964, p. 485-522.

2. Altman, D., "Hybrid Rocket Propulsion, Prospects for the Future", AIAA 50th Anniversary Meeting, May 1981.

3. Calabro, M., "European Hybrid Propulsion History" 29th Aerospace Sciences Meeting, May 10, 1991.

4. Altman, D., "Hybrid Rocket Development History" 27th Joint Propulsion Conference, AIAA/SAE/ASNE June 1991.

5. Karabeyoglu M. A., "Transient Combustion in Hybrid Rockets", Stanford University Ph.D. thesis, August 1998.

6. Karabeyoglu, M. A., B. J. Cantwell and D. Altman "Development and Testing of Paraffin-Based Hybrid Rocket Fuels" 37th AIAA/ASME/SAE/ASEE Joint Propulsion Conference, Salt Lake City, Utah, July 8-11, 2001.

7. Karabeyoglu, M. A., Altman, D. and Cantwell, B. J., "Combustion of Liquefying Hybrid Propellants: Part I General Theory", *AIAA Journal of Propulsion and Power*, Vol. 18, No 3, 2002, p. 610-620.

8. Karabeyoglu, M. A. and Cantwell, B. J. "Combustion of Liquefying Hybrid Propellants: Part II Stability of Liquid Films" *AIAA Journal of Propulsion and Power*, Vol. 18, No. 3, 2002, p. 621-630.

9. Chase, C. A., "IUS Solid Rocket Motors Overview", JANNAF Conference, Monterey, California, February 1983.

10. Sutton, G., "Rocket Propulsion Elements", Wiley-Intescience, Sixth Edition, 1992, p. 512-513.

11. George, P, Krishnan, S. Varkey, P.M. Ravindran, M and Ramachandran, L. "Fuel Regression Rate in Hydroxyl-Terminated-Polybutadiene/Gaseous-Oxygen Hybrid Rocket Motors", *AIAA Journal of Propulsion and Power*, Vol. 17, No. 1, 2001, p. 35-42.

12. Risha, G. A., Boyer E., Wehrman R. B. and Kuo K. K., "Performance Comparison of HTPB-Based Solid Fuels Containing Nano-Sized Energetic Powder in a Cylindrical Hybrid Rocket Motor", 38th AIAA/ASME/SAE/ASEE Joint Propulsion Conference, Indianapolis, Indiana, July 7-10, 2002.

13. Knuth, W., Chiaverini, J., Sauer, A., and Gramer, D.J. "Solid-Fuel Regression Rate Behavior of Vortex Hybrid Rocket Engines", *AIAA Journal of Propulsion and Power*, Vol. 18, No. 3, 2002, p. 600-609.

14. Karabeyoglu, M. A. and Altman, D., "Dynamic Modeling of Hybrid Rocket Combustion", *AIAA Journal of Propulsion and Power* Vol. 15, No 4, 1999, p. 562-571.

15. De Zilwa, S., Zilliac, G., Karabeyoglu, A. and Reinath, M., "Combustion Oscillations in High Regression Rate Hybrid Rockets", Submitted for presentation at the 39th AIAA/ASME/ASEE Joint Propulsion Conference, Alabama, 2003.

16. Ward-Smith, A., J., "Critical Flowmetering: The Characteristics of Cylindrical Nozzles with Sharp Upstream Edges", *International Journal of Heat and Fluid Flow*, Vol. 1 No. 3, p. 123-132, 1979.

17. Miller, W., R., "Flow Measurement Engineering Handbook", McGraw-Hill, Third Addition, NY, 1996.

11) Appendix – Data Reduction Details

Regression Rate

The space-time averaged regression rate for a given test is estimated from initial port diameter and consumed fuel mass measurements. The following relations are used in the calculations.

$$\bar{\dot{r}} = \frac{d_{vc} - d_i}{2\ t_b} \qquad \text{(A1a)}$$

$$d_f = \left[d_i^2 + \frac{4\Delta M_f}{\pi r_f L_g} \right]^{1/2} \qquad \text{(A1b)}$$

Here d_i, d_f are initial and final port diameters, d_{vc} is the port diameter at the start of the thrust termination event, ΔM_f is the total mass of the fuel

burned (i.e. difference of two weight measurements before and after the test) and L_g is the fuel grain length. The fuel density, r_f, is taken to be 0.92 g/cm^2-sec based on independent density measurements. The burn time, t_b, is defined as the time between the ignition and the valve closing events which are illustrated in Figure 13 for the motor test 4P-03. As it is evident from the figure the thrust termination response of the feed system is slow due to the large volume of oxygen feed system piping. Since a significant amount of fuel is consumed during the thrust termination process, the regression rate measurement must be corrected for an accurate characterization of the regression rate behavior. We have developed a correction procedure based on an estimation of the port diameter change during thrust termination transient. For an exponential oxidizer mass flow rate decay function, the relation between the final port diameter and the port diameter at the start of the thrust termination event is determined to be

$$d_{vc} = \left\{ \left[\frac{2n+1}{n} \frac{2^{n+1}}{p^n} t_{fs}\, a\, \dot{m}_{ox}^{ter} \left(1 - e^{-n t_f / t_{fs}} \right) \right] + d_f^{2n+1} \right\}^{1/(2n+1)} \tag{A2}$$

The differential equation relating the port diameter change to the regression rate expression ($\dot{r} = a\, G_{ox}^n$) is integrated to obtain equation A2. Note that a and n are the regression rate coefficient and exponent for the propellant system of interest and $\dot{m}_{ox}^{ter}$ is the oxidizer mass flow rate at the start of the thrust termination event. In equation A2, the characteristic time scale of the feed system is defined as

$$t_{fs} = \frac{V_f}{A_{or} c_{ox}^*}. \tag{A3}$$

Here V_f is the volume of the feed system piping (estimated to be 0.017 m^3), A_{or} is the oxidizer feed system orifice area, c_{ox}^* is the characteristic velocity for the oxygen gas at ambient temperature. For certain testing conditions this characteristic time can be as long as 1.5 seconds, a significant period compared to the nominal burn time of 8 seconds. The time variable, t_f, is defined as the time after the main valve closing event that the fuel regression rate becomes negligible. For all calculations we have used a t_f / t_{fc} ratio of 1.2. It has been determined that the effect of the t_f / t_{fc} ratio on the regression rate correction diminishes significantly for values larger than 1.2 due to the exponential nature of the oxidizer mass flow rate decay.

We also like to note that, unlike the thrust termination transient, the ignition event is fast compared to the overall burn time, making an ignition correction unnecessary.

Oxidizer Mass Flow Rate

The oxidizer mass flow rate is measured by two means: 1) sonic orifice and 2) calibrated venturi, both inserted in the main oxidizer line. For the sonic orifice measurement, with the choked flow assumption (which is valid for the whole duration of the test) the mass flow rate can be expressed as

$$\dot{m}_{ox} = \frac{P_f A_{or} C_D}{c_{ox}^*}. \tag{A4}$$

The discharge coefficient, C_D, for the thick square edge orifice is taken as 0.84 as recommended in Ref. 16. The mass flow calculations for the venturi are based on the equations suggested in Ref. 17. The two mass flow rate measurement methods are determined to be in good agreement for all of the tests (i.e. typically the difference is less than 1%). The only deviation is observed during transients, for which the venturi measurement becomes questionable (since the quasi-steady assumption is violated). The average oxidizer mass flow rate, $\overline{\dot{m}}_{ox}$, is estimated over the course of the burn, from ignition event to the valve closing event.

Oxidizer Mass Flux

It is suggested in the literature[1] that the local instantaneous regression rate of a hybrid fuel depend on the local instantaneous mass flux. However, it is much more convenient to present the regression rate law of a propellant system in terms of the space-time averaged regression rate versus the space-time averaged mass flux. Even though the space-time averaged regression rate is a well-defined quantity, the selection of a particular mass flux averaging method is necessary. For the purposes of this paper we use the oxidizer mass flux based on the averaged port diameter over the course of the run.

$$\overline{G}_{ox} = \frac{16\ \overline{\dot{m}}_{ox}}{p \left(d_i + d_{vc} \right)^2} \tag{A5}$$

It can be shown that the average diameter method (i.e. as opposed to the average area or average flux

methods) results in the most accurate representation of the hybrid regression rate law. The selection of the oxidizer mass flux, G_{ox}, rate over the total mass flux, G_{tot}, is completely arbitrary, since both cases should be corrected for the average O/F ratio of the motor. The correction formula for the oxidizer mass flux case is given in equation 1.

Combustion Efficiency

The combustion efficiency (i.e. c* efficiency) of the motor is calculated based on the following equation:

$$h_c = \frac{c^*_{act}}{c^*_{theo}} \qquad \text{(A6)}$$

The measured characteristic velocity, c^*_{act}, for each test is estimated with use of the following relation.

$$c^*_{act} = \frac{\int_0^{t_b + t_f} P_c dt}{(\Delta M_{ox} + \Delta M_f)\ C_d \overline{A}_n} \qquad \text{(A7)}$$

Note that the pressure integral includes the regular test period and the thrust termination event. Here $\overline{A}_n$ is the average nozzle area, C_d is the nozzle discharge coefficient and ΔM_{ox} is the total oxidizer mass consumed during the regular test and the thrust termination periods. The theoretical characteristic velocity, c^*_{theo}, is evaluated at the average motor $O/F = \Delta M_{ox}/\Delta M_f$. The nozzle discharge coefficient is taken as 0.99 for all tests.

We finally note that for most of motor tests reported in this paper, the total igniter gas mass is less than 30 grams. Thus, the effect of the igniter mass on the regression rate and efficiency measurements is negligible.

12) Tables and Figures

	HTPB-Based Single Circular Port	Paraffin-Based Single Circular Port	HTPB-Based 7+1 WW Port
Fuel Grain Length, m	8.97	3.17	3.12
Fuel Grain OD, m	0.73	1.14	1.20
Fuel Grain L/D	12.22	2.78	2.60
Initial Web Thickness, m	0.23	0.43	0.14
Total Propellant Mass, kg	10,380	10,380	10,380
Burned Fuel Mass, kg	2,971	2,811	2,971
Unburned Fuel Mass, kg	52 (1.8%)	37 (1.3%)	224 (7.5%)
Web Support Mass, kg	0	0	80
Total Unburned Mass, kg	52 (1.8%)	37 (1.3%)	304 (10.2%)
Motor O/F	2.5	2.7	2.5
Initial Ox. Flux, g/sec-cm^2	50	50	50
Total Impulse, M N-sec	33.8	34.1	33.9
Thrust @ Termination, kN	128	130	127
Thrust @ Start, kN	145	145	147
Delivered Isp, sec	331	334	332
O/F Shift	0.85	0.86	1.37
Burn Time, sec	250	250	250

Table 1: System comparisons.

Test	Orifice Diam. (in.)	Initial Port Diam. (in.)	Initial Nozzle Throat Diam. (in.)	Actual Burn Time (sec)	Notes
ST	0.56	3.972	1.98	7.00	Cracked fuel grain
4F-2	0.45	3.620	1.45	9.25	Nozzle failure
4F-1	0.45	4.412	1.46	9.35	Successful Test
4F-2a-1	Premature shutdown- software failure. No data reduction.				
4F-2a-2	Fuel grain of 4F-2a-1 is re-fired. No data reduction.				
4F-1a	0.56	5.098	1.98	7.60	Nozzle erosion/Good test
4F-4	0.56	3.943	1.98	8.50	Nozzle erosion/Good test
4F-5	0.56	3.591	1.98	8.20	Nozzle erosion/Good test
4F-3	Injector fire. No data reduction.				
4F-1b	0.45	4.415	1.45	9.50	Successful Test
4Thr-1	0.45	3.501	1.45	10.50	Successful Test/Throttling
4F-1c	0.45	5.131	1.45	10.35	Successful Test
4F-3a	0.56	4.464	1.98	8.30	Successful Test
4L-01	0.56	4.450	1.98	8.45	Successful Test
4P-01	0.56	4.482	2.80	8.40	Successful Test
4P-02	0.56	4.600	1.62	7.25	Successful Test
4P-03	0.56	4.423	1.62	8.25	Successful Test
4L-03	0.56	5.536	1.98	6.20	Successful Test
4L-04	0.56	3.517	1.98	8.30	Successful Test
4L-05	0.56	3.941	1.98	8.25	Successful Test
4L-06	0.56	3.009	1.98	8.20	Fuel Port Failure
4L-07	0.56	2.968	2.040	8.00	Fuel Port Failure
4L-08	0.56	4.055	2.212	8.15	Successful Test
4I-01	0.56	4.434	2.808	8.25	Successful Test
4P-04	0.45	4.433	2.817	8.15	Successful Test
4L-09	0.56	3.544	2.190	8.15	Successful Test
4L-10	0.68	4.454	2.415	8.20	Successful Test
4L-11	0.56	6.057	2.020	2.55	Control System Failure
4L-12	0.45	4.055	2.020	7.30	Successful Test

Table 2: Motor test conditions and notes.

Test	Oxidizer mass flow rate (kg/sec)	Initial oxidizer flux, (g/cm^2-sec)	Average oxidizer flux, (g/cm^2-sec)	Regression rate, (mm/sec)	O/F	Chamber pressure, (psi)	C* efficiency
ST	2.07	27.12	16.66	3.59	2.18	307	0.78
4F-2	2.06	31.65	18.33	3.09	2.67	163	-
4F-1	2.03	20.87	14.47	2.40	3.05	527	0.85
4F-2a-1	Premature shutdown- software failure. No data reduction.						
4F-2a-2	Fuel grain of 4F-2a-1 is re-fired. No data reduction.						
4F-1a	4.02	-	21.75	3.37	3.89	501	0.91
4F-4	4.24	-	30.92	4.04	3.97	527	0.90
4F-5	4.32	64.32	33.89	4.69	3.54	551	0.88
4F-3	Injector fire. No data reduction.						
4F-1b	2.13	21.58	14.22	2.65	2.72	562	0.85
4Thr-1	1.56	35.00	13.76	2.97	2.02	417	0.77
4F-1c	2.07	15.88	11.45	2.15	3.00	542	0.89
4F-3a	4.39	44.89	27.13	3.90	3.84	568	0.90
4L-01	4.40	44.49	27.05	3.66	2.57	671	0.88
4P-01	4.43	44.36	27.41	3.52	2.69	318	0.82
4P-02	4.42	39.23	26.96	3.82	2.48	994	0.87
4P-03	4.41	43.31	27.88	3.58	2.65	939	0.88
4L-03	4.45	29.11	22.05	3.18	2.69	642	0.84
4L-04	4.44	72.46	36.80	4.17	2.66	657	0.85
4L-05	4.43	57.57	32.44	3.84	2.72	649	0.85
4L-06	4.40	98.80	36.87	5.72	1.97	679	0.80
4L-07	4.43	102.73	33.77	6.73	1.63	652	0.80
4L-08	4.42	54.32	31.29	3.82	2.64	525	0.85
4I-01	4.47	43.62	26.76	4.02	2.40	319	0.78
4P-04	2.11	22.79	14.69	2.74	1.78	159	0.78
4L-09	2.05	32.85	19.21	3.26	1.70	265	0.80
4L-10	5.55	55.25	34.66	4.25	2.89	590	0.88
4L-11	1.47	8.68	7.43	2.00	1.56	213	0.78
4L-12	2.08	11.06	9.40	1.96	2.01	301	0.79

Table 3: Motor test results.

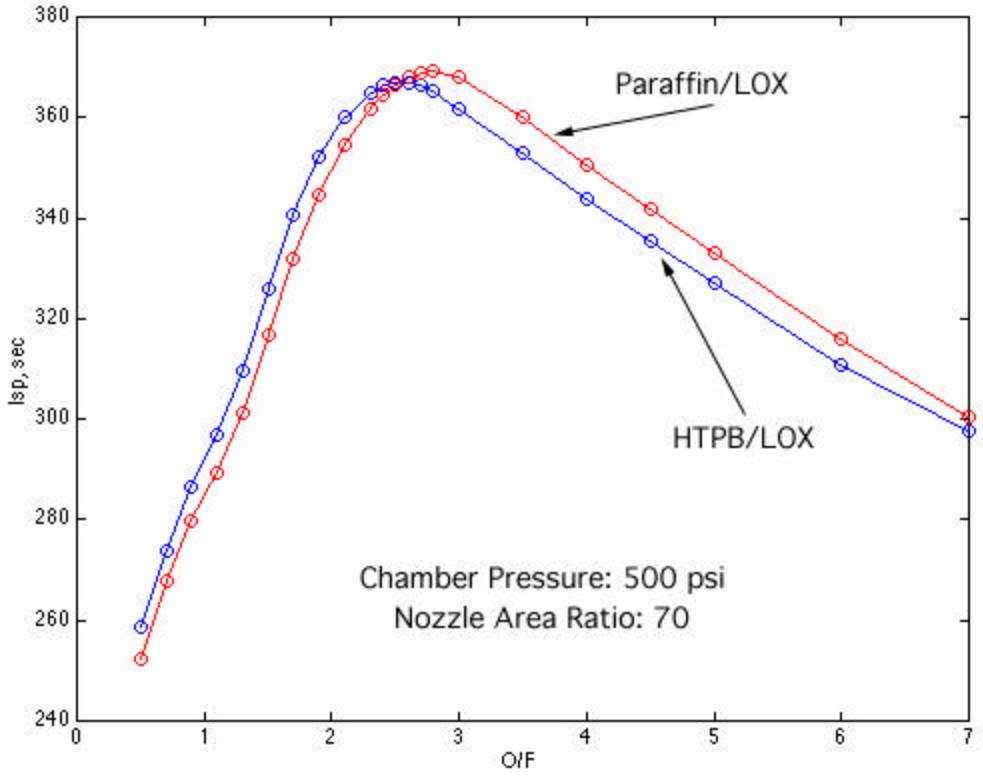

Figure 1: Theoretical Isp performance of the Paraffin/LOX and HTPB/LOX at a chamber pressure of 34 atm (500 psi) and nozzle area ratio of 70.

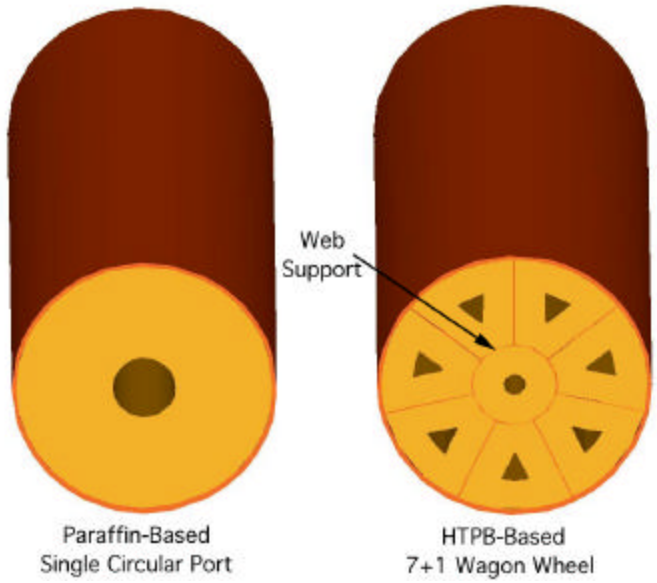

Figure 2: Effect of regression rate on the fuel grain design.

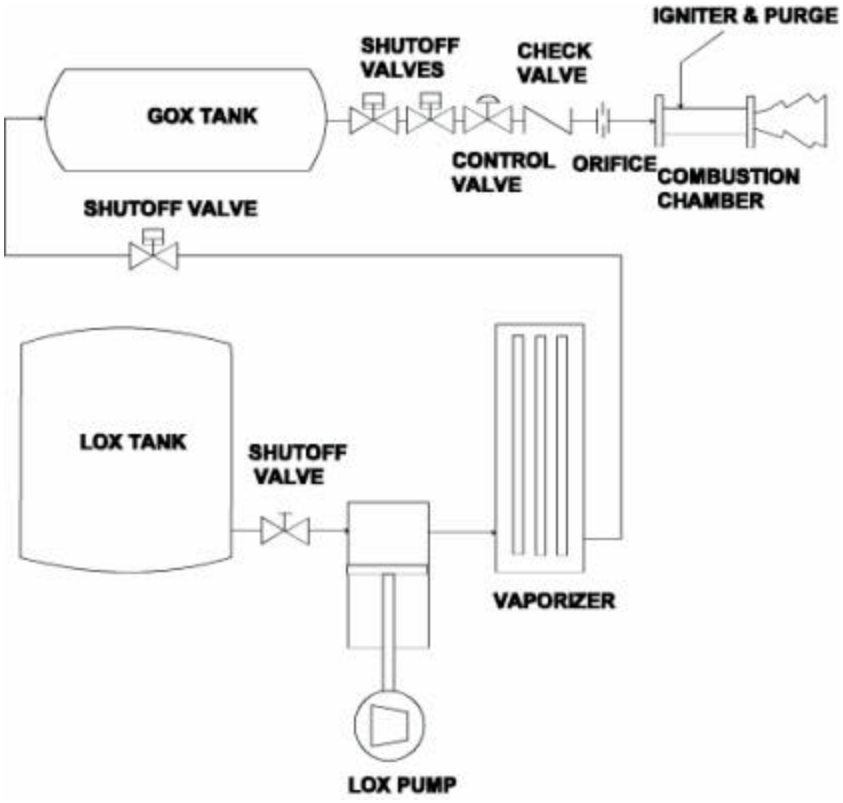

Figure 3: Simplified schematic of the Ames Hybrid Combustion Facility.

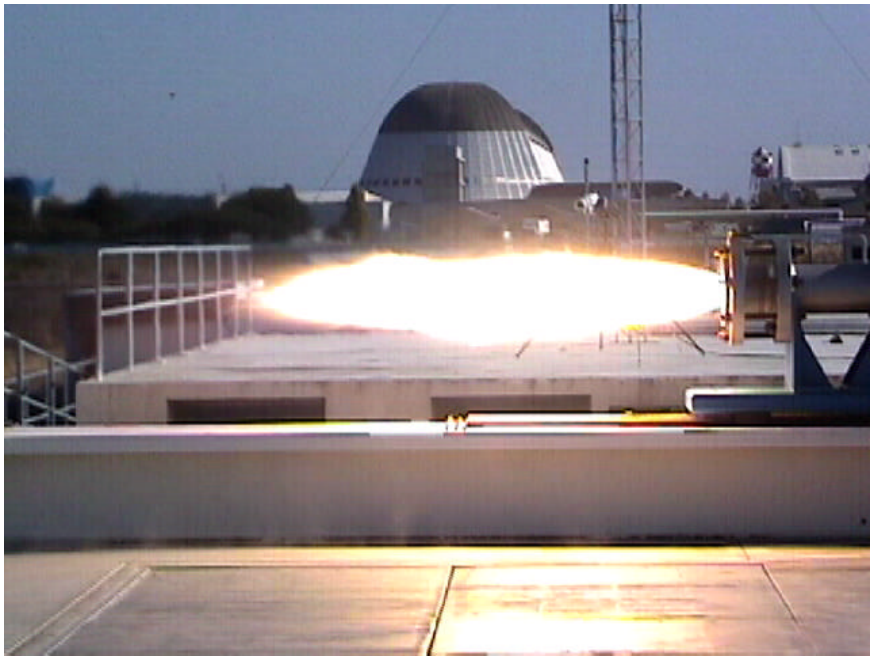

Figure. 4: Ames Hybrid Combustion Facility, first firing.

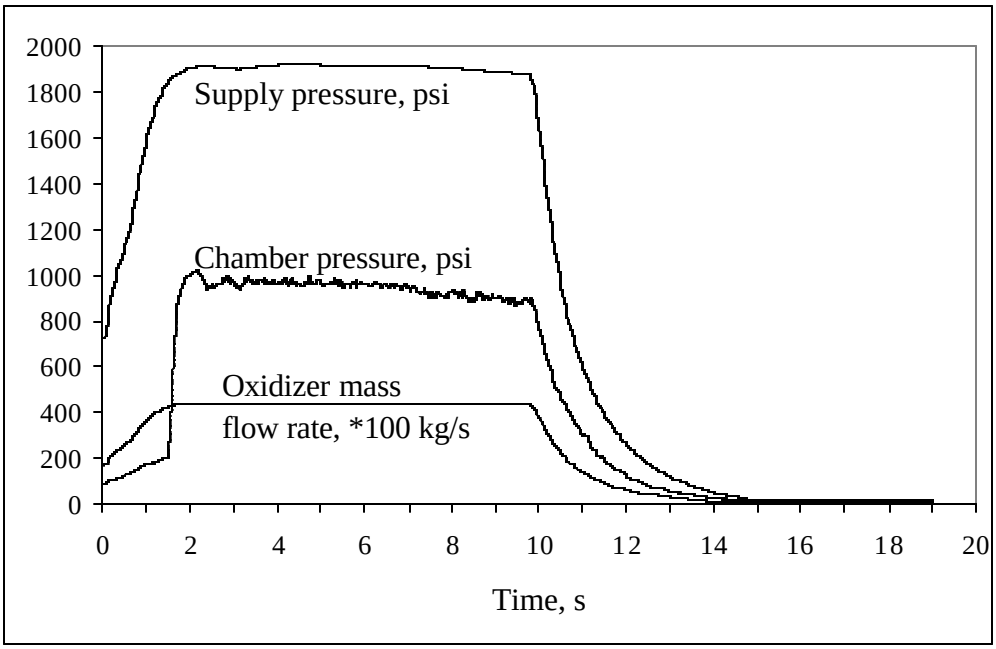

Figure 5: Time histories of chamber pressure and oxygen mass flow rate from a typical run.

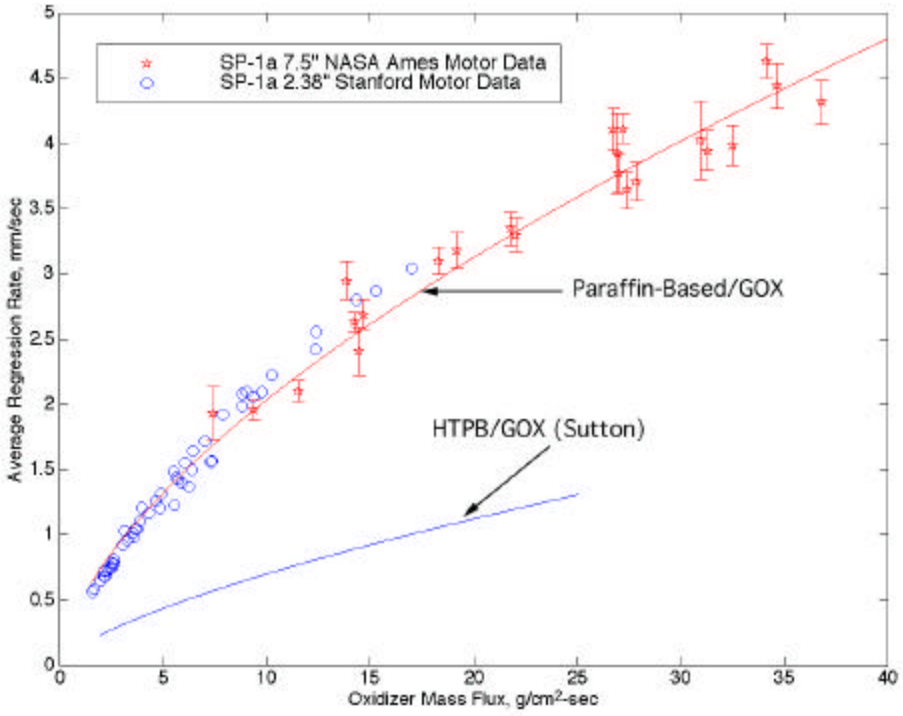

Figure 6: Regression rate data for the paraffin-based fuel, SP-1a.

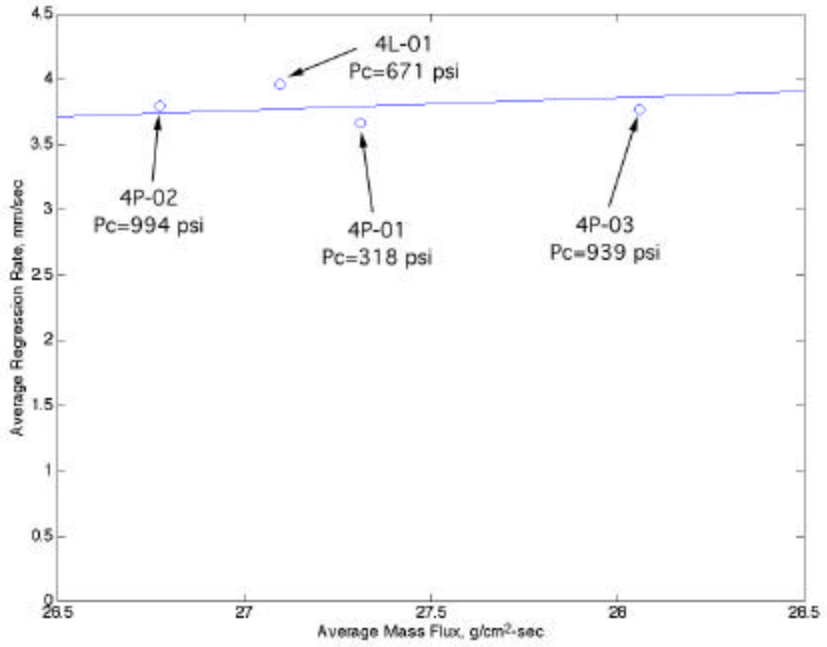

Figure 7: Effect of chamber pressure on the regression rate behavior for paraffin-based propellant SP-1a.

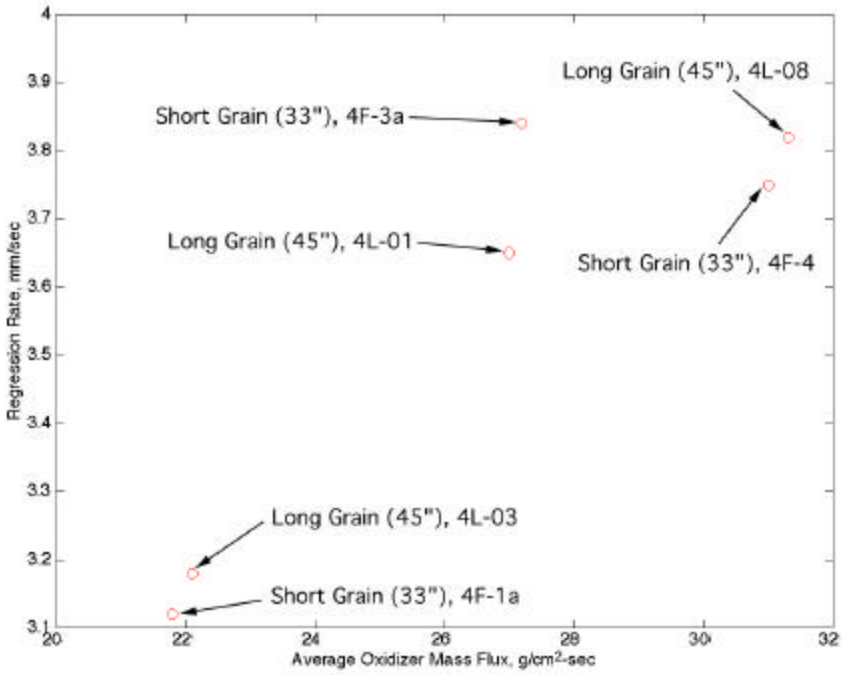

Figure 8: Effect of fuel grain length on the regression rate behavior for paraffin-based propellant SP-1a.

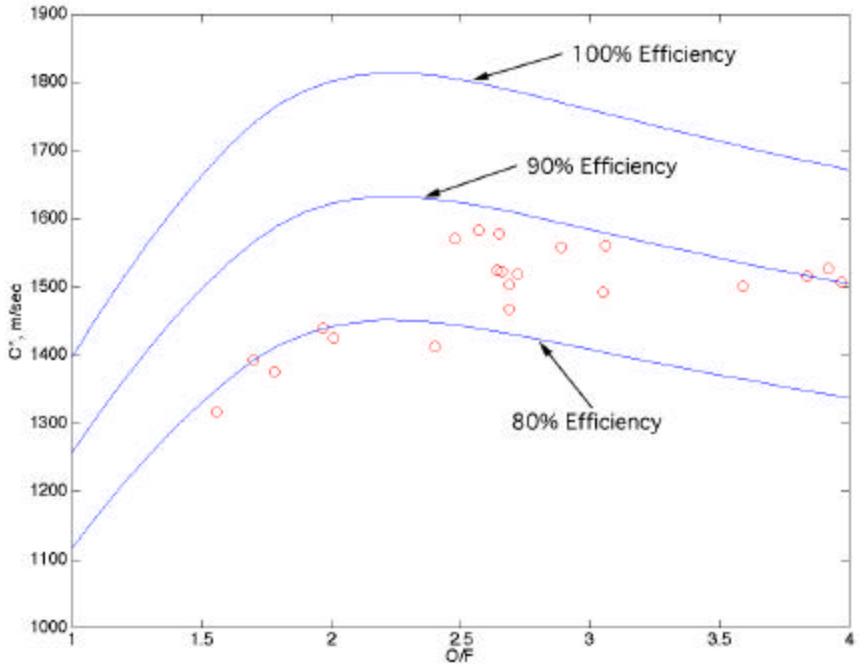

Figure 9: Motor delivered c* as a function of O/F.

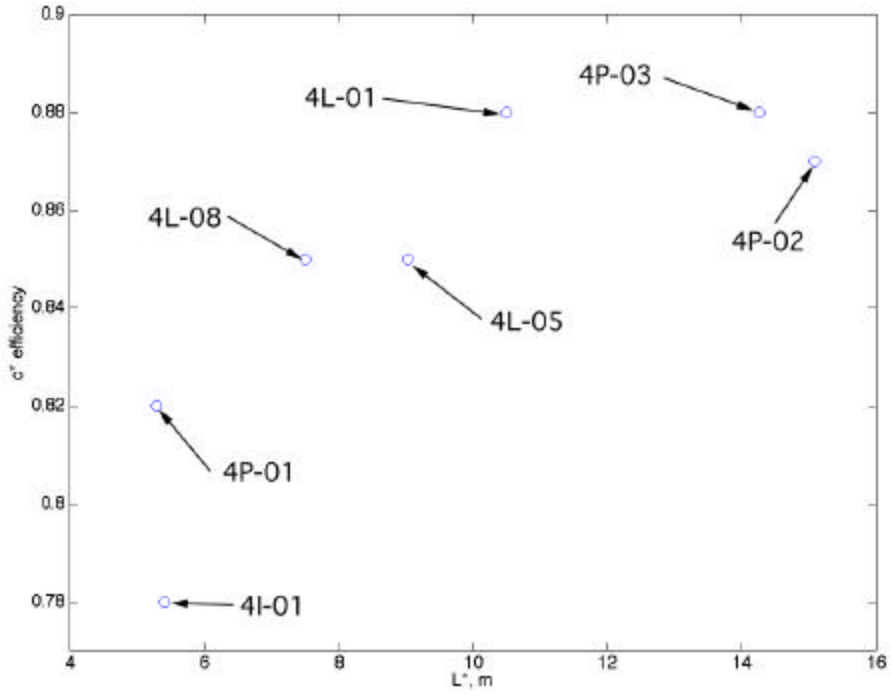

Figure 10: Motor c* efficiency as a function of motor L*.

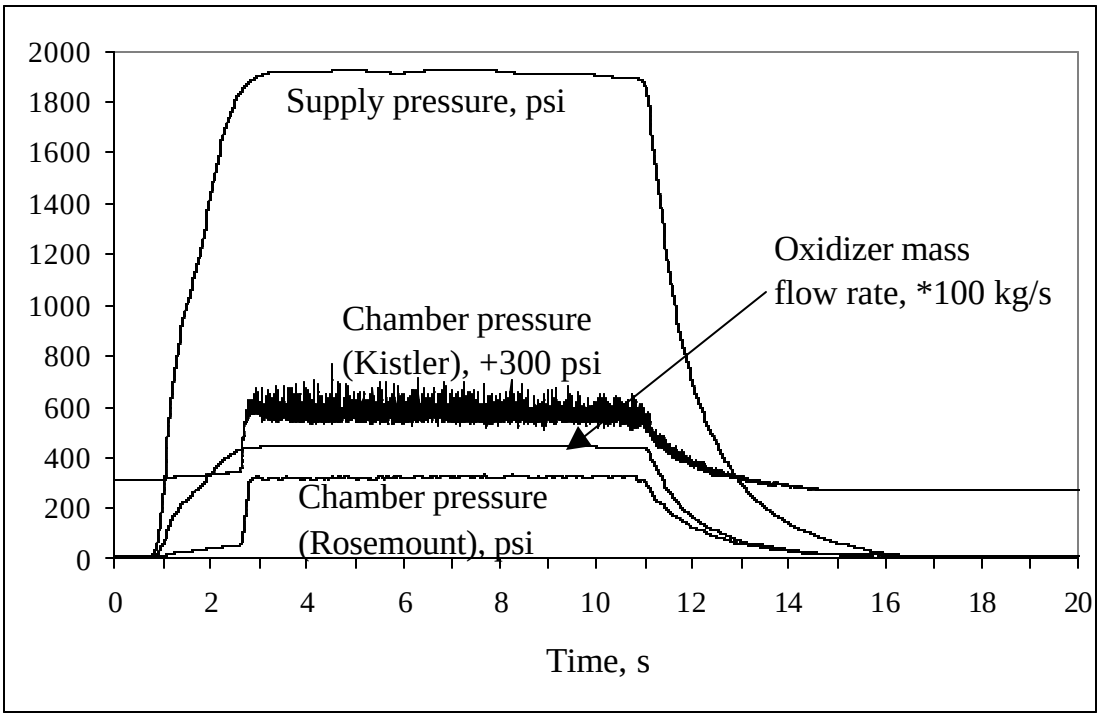

Figure 11: Data acquired during operation for test 4P-01.

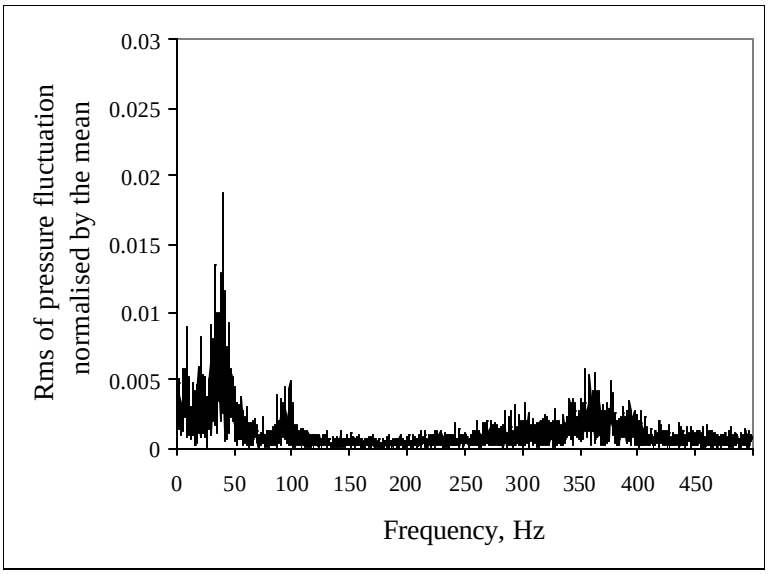

Figure 12: Pressure spectrum for test 4P-01.

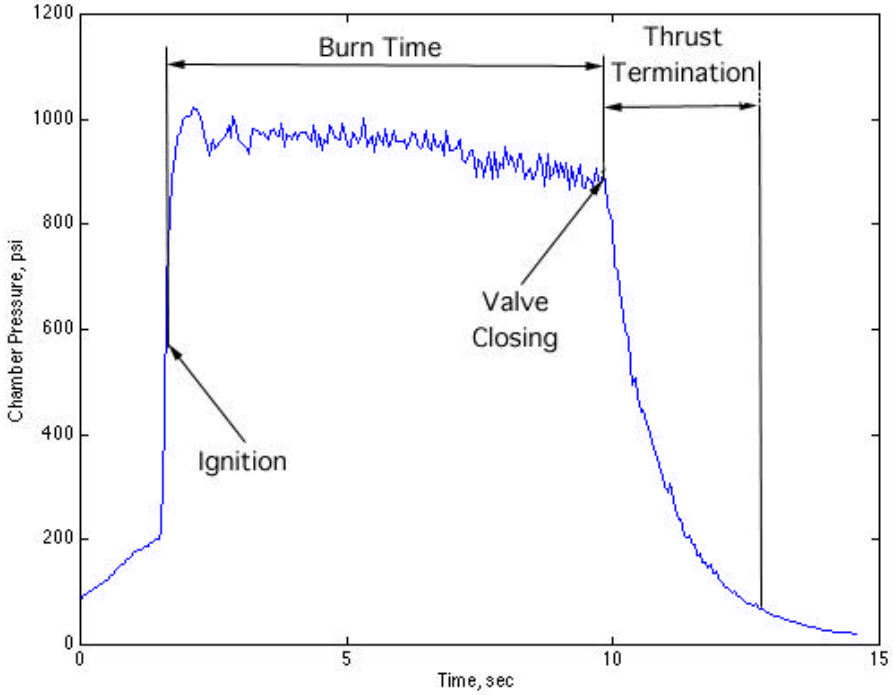

Figure 13: Chamber pressure-time trace for the run 4P-03.